Across Membrane Communication between the Q_o and Q_i Active Sites of Cytochrome bc_1[†]

Jason W. Cooley,[‡] Dong-Woo Lee, and Fevzi Daldal*

Department of Biology, Plant Science Institute, University of Pennsylvania, Philadelphia, Pennsylvania 19104

Received December 3, 2008; Revised Manuscript Received January 14, 2009

ABSTRACT: The ubihydroquinone:cytochrome *c* oxidoreductase (cyt bc_1) contains two catalytically active domains, termed the hydroquinone oxidation (Q_o) and quinone reduction (Q_i) sites, which are distant from each other by over 30 Å. Previously, we have reported that binding of inhibitors to the Q_i site on one (*n*) side of the energy-transducing membrane changes the local environment of the iron−sulfur (Fe/S) protein subunit residing in the Q_o site on the other (*p*) side of the lipid bilayer [Cooley, J. W., Ohnishi, T., and Daldal, F. (2005) *Biochemistry 44*, 10520−10532]. These findings best fit a model whereby the Q_o and Q_i sites of the cyt bc_1 are actively coupled in spite of their distant locations. Because the Fe/S protein of the cyt bc_1 undergoes a large-scale (macro) domain movement during catalysis, we examined various macromobility-defective Fe/S subunit mutants to assess the role of this motion on the coupling of the active sites and also during the multiple turnovers of the enzyme. By monitoring the changing environments of the Fe/S protein [2Fe-2S] cluster upon addition of Q_i site inhibitors in selected mutants, we found that the Q_o−Q_i site interactions manifest differently depending on the ability of the Fe/S protein to move between the cytochrome *b* and cytochrome c_1 subunits of the enzyme. In the presence of antimycin A, an immobile Fe/S protein mutant exhibited no changes in its EPR spectra. In contrast, mobility-restricted mutants showed striking alterations in the EPR line shapes and revealed two discrete subpopulations in respect to the [2Fe-2S] cluster environments at the Q_o site. These findings led us to conclude that the mobility of the Fe/S protein is involved in its response to the occupancy of the Q_i site by different molecules. We propose that the heterogeneity seen might reflect the distinct responses of the two Fe/S proteins at the Q_o sites of the dimeric enzyme upon the occupancy of the Q_i sites and discuss it in terms of the function of the dimeric cyt bc_1 during its multiple turnovers.

The ubihydroquinone (QH_2):cytochrome (cyt)[1] *c* oxidoreductases (cyt bc_1) are crucial enzymes for membrane-associated electron transport pathways implicated in ATP production in mitochondria and most bacteria (*1*−*3*). Similar enzymes are also found in chloroplasts. Available structures at atomic scale resolution of various members of this enzyme family show that they are dimeric multisubunit proteins, with each monomer formed of three ubiquitous, catalytically active subunits (*4*−*9*) (Figure 1). These proteins are the cyt *b* (with two *b*-type hemes, b_H and b_L), cyt c_1 (with a *c*-type heme), and the iron−sulfur (Fe/S) protein subunit with a high potential [2Fe-2S] cluster (*2, 3*). A unique feature of the dimeric cyt bc_1 is the intertwined architecture of its monomers. The cyt *b* and cyt c_1 subunits are fully confined to each monomer while the Fe/S protein spans across both monomers. Each monomer contains the [2Fe-2S] cluster bearing the extrinsic domain of one and the transmembrane helical anchor of the other Fe/S protein (*4*−*9*) (Figure 1). This unusual subunit arrangement is thought to stabilize and structurally interconnect the two monomers together, but its functional importance, if any, remains unclear (*2*).

The catalytic cycle of the cyt bc_1 is described via the modified Q-cycle mechanism, usually without taking into consideration the dimeric state of the enzyme (*3, 10*). The Q-cycle mechanism involves the consecutive oxidation of two QH_2 molecules at a catalytic site, called Q_o, located at the positive (*p*) side of the energy transducing membrane at the interface between the Fe/S protein and cyt *b* subunits (*1, 11, 12*). Each QH_2 oxidation is initiated by an oxidized, high redox potential Fe/S protein, which moves via a tethered rotational displacement (macromovement) after its reduction from the surface of cyt *b* to near the cyt c_1. Following this motion, the reduced [2Fe-2S] cluster equilibrates with the oxidized cyt c_1, completing the conformation-assisted electron transfer event (Figure 1). The high potential electron transport chain, formed of the Fe/S protein and the cyt c_1, then conveys one of the two electrons that originate from QH_2 oxidation to electron carrier cyts *c* (cyt c_2 or cyt c_y in *Rhodobacter capsulatus*) (*13*). These electron carriers then transfer electrons to the photochemical reaction center (RC) or the cyt *c* oxidase (C_{ox}) in photosynthesis or respiration, respectively. The second electron derived from each QH_2

[†] This work was supported by NIH Grant R01 GM 38237 to F. D. and AHA Fellowship 0425515U to J.W.C.

* To whom correspondence should be addressed. Phone: (215) 898-4394. Fax: (215) 898-8780. E-mail: fdaldal@sas.upenn.edu.

[‡] Present address: Department of Chemistry, University of Missouri, Columbia, MO 65211.

[1] Abbreviations: cyt bc_1, ubihydroquinone:cytochrome *c* oxidoreductase; EPR, electron paramagnetic resonance; Fe/S, iron−sulfur; Q_o, hydroquinone oxidation; Q_i, quinone reduction; SQ, semiquinone; Ant, antimycin A; HQNO, 2-*n*-heptylhydroquinoline *N*-oxide; Stig, stigmatellin; MPYE, mineral−peptone−yeast extract; QH_2, hydroquinone; Q, quinone; MOPS, 4-morpholinepropanesulfonic acid.

10.1021/bi802216h CCC: $40.75
Published on Web 02/16/2009

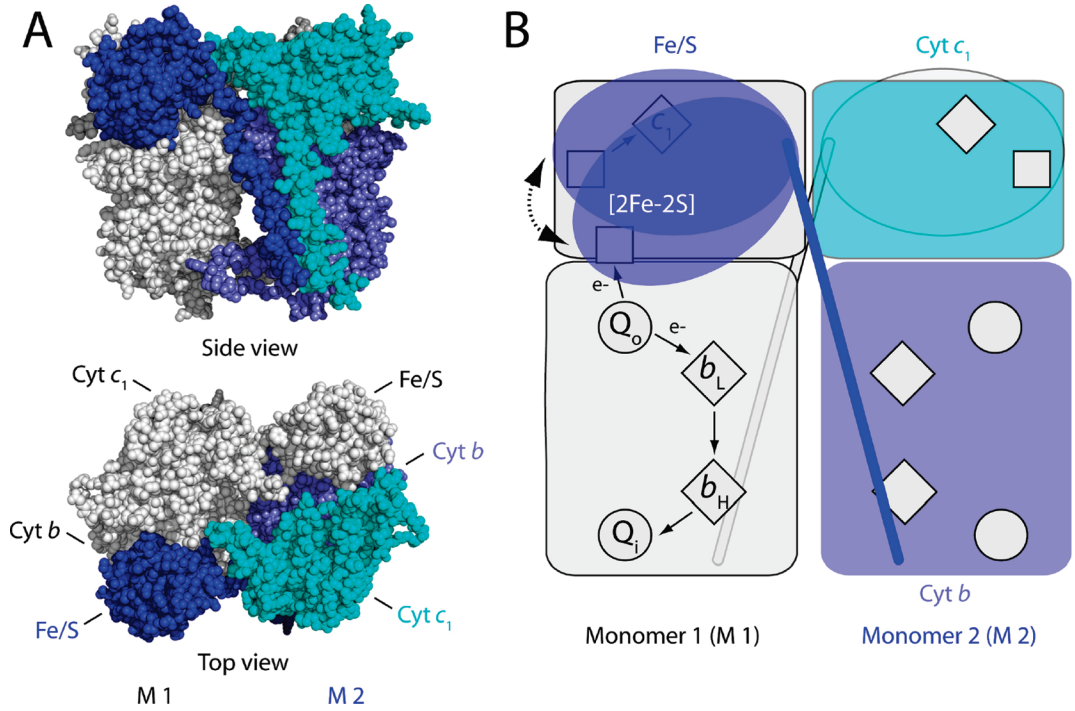

FIGURE 1: Structure of the dimeric cyt bc_1 from *R. capsulatus* and its components. (A) Both a side view (top) and a top view (bottom) of the dimeric cyt bc_1 are shown using space-filling representations. Three subunits of one monomer (M2, right) representing the cyt *b*, the cyt c_1, and the Fe/S protein are in slate, cyan, and blue, whereas those of the other monomer (M1, left) are in white and gray. (B) Modified Q-cycle mechanism of cyt bc_1. The three catalytic subunits (cyt *b*, cyt c_1, and Fe/S), the cofactors (hemes b_L, b_H, and c_1, shown as diamonds, and the [2Fe-2S] cluster as a square), and the active sites (Q_o and Q_i, shown as circles) of the cyt bc_1 are represented schematically. Electron transfer (e^-) steps catalyzed by the enzyme via the bifurcation reaction at the Q_o site are shown with black arrows on the monomer 1(M1) only. The dashed arrows refer to the mobility of the extrinsic domain of the Fe/S protein.

oxidation at the Q_o site equilibrates with a low potential electron transport chain formed by the two *b* (b_L and b_H for low and high potential with respect to one another) hemes of cyt *b*, due to the high degree of instability of the semiquinone (SQ) species at the Q_o site (*14*−*16*). This second electron reduces a quinone (Q) residing at another catalytic site of the enzyme, called the Q_i site, to a temporally stable SQ. Upon a subsequent turnover of a Q_o site, the SQ is converted to a QH_2 and released from the enzyme (Figure 1). The Q_i site is defined by residues deriving from the cyt *b* subunit and its cofactors and is located about 30 Å away from the Q_o site across the lipid bilayer, on the negative (*n*) side of the membrane (*6, 8*). Conveying the two electrons emanating from QH_2 oxidization to two separate electron transport chains with different thermodynamic properties via a "bifurcated" mechanism is central to the efficiency of the cyt bc_1 (*11, 17*).

Despite the availability of several atomic scale structures with various Q_i site occupants (*7, 18*) less is known about the events that separate completion of the first QH_2 oxidation and initiation of the second QH_2 oxidation during a complete catalytic cycle of the cyt bc_1 (*19*). Similarly, how the subsequent catalytic cycles are conducted to ensure the steady-state turnover of the cyt bc_1 is not clear. How does the enzyme coordinate the stabilization of a SQ at a Q_i site with the initiation of a second QH_2 oxidation (*20*)? Does it use the Q_o site of the same monomer consecutively, or does it alternate between the Q_o sites of two monomers (*21, 22*), or does it operate randomly (*23*)? Earlier works indicated that tight interactions between specific residues of the extrinsic domain of the Fe/S protein and cyt *b* (i.e., *cd*1 and *cd*2 helices and *ef* loop) are important for proper Q_o site catalysis (*19, 24*). More recent structural analyses proposed that these interactions might act as a "gate" for holding or releasing the Fe/S protein on the cyt *b* surface at the Q_o site (*8, 25*). However, it remains unclear whether the occupants of the Q_o site or the docking of the Fe/S protein to cyt *b* induces these changes.

Compromising the mobility of the Fe/S protein renders the cyt bc_1 nonfunctional, but a macromovement-defective enzyme can still catalyze a single bifurcated QH_2 oxidation efficiently through a "cyt $b-QH_2-$oxidized Fe/S subunit" ternary complex at the Q_o site (*19*). However, multiple turnovers do not take place, indicating that the Fe/S protein mobility is required for multiple QH_2 oxidations (*26*−*28*). Aside from various mutational or "occupancy" changes at the Q_o site, occupants or mutations at the distant Q_i site also affect the mobility of the Fe/S protein (*21, 29, 30*). A striking example is the inhibition of the cyt bc_1 by the Q_i site antimycin A, where the yield of QH_2 oxidation is one-half of that observed with the uninhibited enzyme (*31, 32*). Even if additional QH_2 oxidations are allowed in the presence of antimycin A, no further cyt *b* reduction occurs. Instead, the second electron from such QH_2 oxidation is usually conveyed to other acceptor molecules (e.g., molecular oxygen) via energetically unfavorable "bypass" reactions at rates of about 1% of the uninhibited Q_o site catalysis (*14, 33*). Coordination of the Q_o-Q_i site catalysis appears to be an intrinsic property of the cyt bc_1 for the onset of multiple QH_2 oxidations. However, how this coordination occurs, and to what extent the structural elements of the enzyme are important for this regulation, remains unclear.

Previously, we have reported that specific interactions of individual cyt *b* residues at the Q_i site with various molecules

bound at this site significantly influence the Q_o site associated environment of the Fe/S protein. The occurrence of these Q_i-mediated Fe/S protein changes is independent of the intactness of the low potential redox chain, and the nature of these changes is variable depending on the molecule occupying the Q_i site (*20*). Specifically, orientation-dependent EPR spectroscopy and ordered membrane samples revealed distinct effects with different Q_i site occupants on the environment of the reduced [2Fe-2S] cluster at the Q_o site (*20*). In the presence of 2-*n*-heptylhydroxyquinoline *N*-oxide (HQNO), which is a potent Q_i site inhibitor, the EPR line shape of the Fe/S protein was altered significantly, but its relative mobility was unchanged. In contrast, in the presence of antimycin A both the line shape and mobility of the Fe/S protein were altered, yielding orientation-independent EPR spectra with otherwise similarly ordered membrane samples. Here, we have extended these observations to various Fe/S protein mobility-defective mutants carrying insertion mutations (+*n*Ala) in the hinge region of this subunit (*20, 34*) to ascertain whether the Q_i site occupancy by antimycin A would alter the orientation dependence of the [2Fe-2S] cluster EPR spectra as a consequence of the Fe/S protein mobility. We have found that upon antimycin A addition immobile mutants (i.e., lacking both the micro- and macromobility of the Fe/S protein) did not show any change, and mobility-restricted mutants exhibited specific changes that were dissipated in suppressor mutants correcting the mobility defects. In addition, exposure of the macromobility-hindered +1Ala and macromobility-abolished +2Ala insertion mutants to antimycin A yielded a remarkable partitioning of the EPR g_x transition maxima to two distinct magnetic field positions within the same spectra, suggesting that the two Fe/S proteins of the dimeric cyt bc_1 might have their [2Fe-2S] clusters in different environments. These findings raised the possibility that the cyt bc_1 might function as a catalytically heterodimeric enzyme, and herein we discuss how such asymmetry may influence the mechanism of multiple turnovers of the enzyme.

MATERIALS AND METHODS

Bacterial Strains and Growth Conditions. R. capsulatus strains were grown in mineral−peptone−yeast extract enriched media (MPYE) under semiaerobic conditions in the dark at 35 °C, as described previously (*35*). The construction, growth phenotypes, and biophysical−biochemical characterizations of the +1Ala, +2Ala, and +3Ala cyt bc_1 mutants and their double mutant derivatives (+*n*Ala-bH212N and +*n*Ala-bL286F) have been described previously (*19, 33, 34*), with the exception of the +1Ala-bH212N double mutant, which was constructed in a manner similar to that of the +2Ala-bH212N double mutant (*33*).

Preparation and Spectroscopic Analysis of Ordered Membrane Samples. Chromatophore membranes were prepared as described previously in ref *35*. Ordered membrane sample preparation was as described in refs *36* and *37*. Using membrane samples, EPR spectra were recorded between angles of 0° and 180° from the magnetic field vector using 10° rotational steps. EPR spectroscopy was carried out at sample temperatures of 20 K on a Bruker ESP 300E spectrometer (Bruker Biosciences Inc.) fitted with an Oxford instruments ESR-9 helium cryostat (Oxford Instrumentation Inc.). Additional spectrometer settings were as indicated in figure legends. For orientation-dependent spectral acquisition a goniometer of homemade design, adequate for consistent reproduction of angular values with ±2.5° precision, was utilized. Antimycin A and HQNO (Sigma-Aldrich, Inc.) stock solutions were prepared in dimethyl sulfoxide and used, except where noted, at 10 and 30 μM final concentrations, respectively, per approximately 30 mg/mL total chromatophore membrane proteins prior to drying the membranes. Chemical reduction of the samples was achieved by addition of sodium ascorbate (Sigma-Aldrich, Inc.) to 5 mM final concentrations, and EPR samples were stored in liquid N_2 until spectra were recorded.

Absence of binding of antimycin A or HQNO to the Q_o site of the cyt bc_1 in chromatophore membranes was monitored using light-activated kinetic spectroscopy as performed earlier (*29, 38*), except that cyt *b* reduction kinetics were also measured in the presence of a very large excess (50−200 μM) of Q_i site inhibitors as needed.

RESULTS

Effects of Antimycin A on the Environment of the [2Fe-2S] Cluster in Cyt bc_1 Mutants with Mobility-Impaired Fe/S Proteins. Our previous work indicated that exposure of native cyt bc_1 to antimycin A significantly modified the Fe/S subunit [2Fe-2S] cluster EPR spectra (*20*). Both the line shape and transition maxima of the spectra were changed, and the angular dependence of the EPR transitions was abolished. As the layered membrane samples used were equivalently ordered, these findings indicated that binding of antimycin A induced changes in the steady-state position of the Fe/S protein due to its mobility within the cyt bc_1 (*20*) (reproduced here in Figure 2, top row). In this work, we have examined the cyt bc_1 mutants with impaired Fe/S protein mobility (+*n*Ala mutants) to define their effects on EPR spectral modifications. The cyt bc_1 +*n*Ala mutants contain one, two, or three alanine residue insertions at position 46 of the hinge region of the Fe/S subunit. Based on cyt *c* rereduction kinetics, these mutants exhibit either slow (>millisecond range; i.e., slow macromovement and normal micromovement), very slow (∼second range; i.e., no macromovement but normal micromovement), or undetectable (∼minute range; i.e., no macro- nor micromovements) Fe/S protein mobility, respectively (*34, 36*). In the absence of antimycin A, equivalently ordered membrane samples of +1Ala and +2Ala mutants exhibited EPR spectra that were highly similar to those of native cyt bc_1 in respect to their spectral shapes and angular dependences with the exception that the high-field shoulders were broader than in the native untreated spectra (Figure 2A). The notable difference among the mutants examined was seen with +3Ala mutant derived ordered membrane EPR spectra, which exhibited a narrower and more symmetric g_x transition than the other mutants and the native enzyme (Table 1). In all cases, the g_x transition maxima were similar to that of the native enzyme, centered at $g = 1.805$, typically interpreted as indicative of interactions of the reduced [2Fe-2S] cluster with a Q residing at the Q_o site (*39*).

In the presence of antimycin A, the EPR spectra obtained with +*n*Ala mutant derived ordered membrane samples varied significantly from those obtained from the native

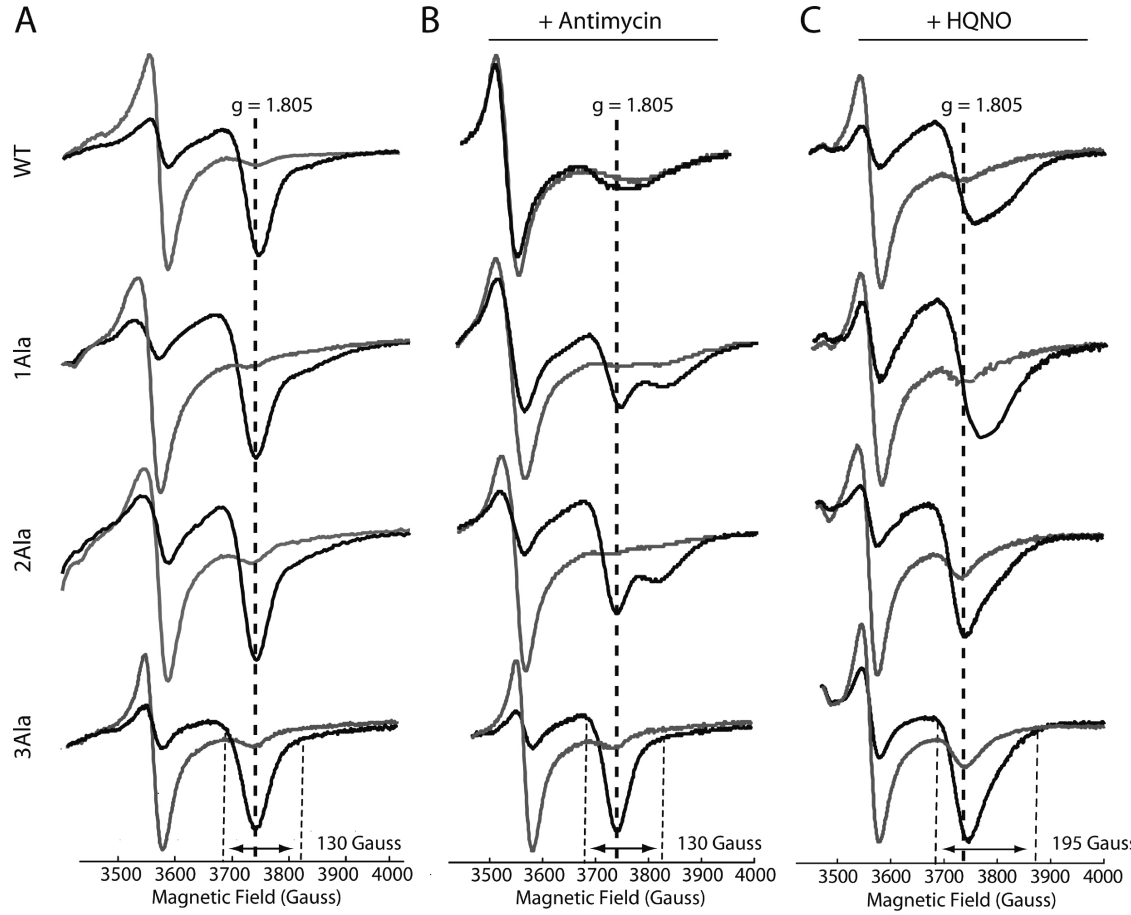

FIGURE 2: Orientation-dependent EPR spectra of the [2Fe-2S] cluster of the Fe/S protein using ordered membranes derived from wild-type and +*n*Ala cyt bc_1 containing strains in the absence or presence of Q_i site inhibitors. Spectra obtained using ordered membranes of a wild-type strain (upper row) (taken from ref *20*) and of +1Ala (second row), +2Ala (third row), and +3Ala (bottom row) mutants, in the absence of inhibitor (A, left) and in the presence of antimycin A (10 μM) (B, middle) or HQNO (30 μM) (C, right) are shown. Spectra acquired at orientations versus the magnetic field where the g_y (gray traces) or g_x (black traces) transition amplitudes were maximal are shown. For the spectra obtained with the +3Ala samples the width of the transitions in the g_x region is indicated to compare the changes in similar spectral shapes. Membranes were prepared as described in the Materials and Methods, and the EPR spectra were recorded at 20 K, 9.443 ± 0.002 GHz microwave frequencies attenuated to 2 mW of power with modulation amplitudes of 12 G.

enzyme and were also distinct from one another (Figure 2B). Unlike the native enzyme, pronounced angular dependence of EPR spectra was observed with the +*n*Ala mutants, whereas in the case of the immobile +3Ala mutant no change was seen with the addition of antimycin A. Thus, the native macromobility of the Fe/S protein was required for the loss of the angular dependence of the EPR spectra caused by exposure to antimycin A. Interestingly, in the +1Ala and +2Ala mutants, antimycin A induced an additional g_x-like transition maximum, termed here g_x', at a higher magnetic field sweep (Figure 2B). The additional g_x' transitions were at $g = 1.765$ and $g = 1.770$ in the +1Ala and +2Ala mutants, respectively (Table 1). This suggested that a second subpopulation of [2Fe-2S] clusters exploring a different environment became more prominent when the mobility-impaired Fe/S proteins were exposed to antimycin A. The g_x' transition was barely seen with the native cyt bc_1 and not with the immobile +3Ala mutant, suggesting that restricted mobility of the Fe/S protein was needed to expose clearly this second subpopulation (Figure 2B). The g_x' transition values were more similar to those seen with UQ-extracted, or myxothiazol-inhibited, cyt bc_1 containing membranes, where the [2Fe-2S] clusters of Fe/S proteins are thought to be more solvent exposed and less buried into the cyt *b* Q_o site than those producing the $g_x = 1.805$ transitions (i.e., [2Fe-2S] clusters that are buried in the solvent-excluded, UQ-containing Q_o site) (*39*).

Effects of HQNO on the Environment of the [2Fe-2S] Cluster in Cyt bc_1 Mutants with Mobility-Impaired Fe/S Proteins. Previously we had observed that, unlike antimycin A, the Fe/S protein [2Fe-2S] cluster EPR spectra of the native enzyme still exhibited their native enzyme-like angular dependence in the presence of HQNO (*20*). Whether this was also the case with the mobility-defective +*n*Ala mutants of cyt bc_1 was also examined (Figure 2C). Adding HQNO broadened the EPR spectra of all +*n*Ala mutants, reflecting the previously observed changes that occurred in the immediate surrounding of the [2Fe-2S] clusters at the Q_o site. However, angular dependences of the EPR spectral transitions were not observably changed, and unlike antimycin A, no additional g_x'-like transition was seen with either the +1Ala or +2Ala mutants. In the case of the +3Ala mutant the $g_x = 1.805$ transition was significantly broadened (approximately 130 versus 190 G) as compared with native or antimycin A treated ordered membrane samples (Figure 2, last row) (Table 1). Restricting the mobility of the Fe/S protein did not yield any spectrally discrete g_x maxima subpopulations of the [2Fe-2S] clusters of the cyt bc_1 upon addition of HQNO, again indicating that different Q_i site

Table 1: EPR *g* Transition Positions and Spectral Widths from Various Single Mutant Ordered Membrane Samples

	transition maxima		transition width	
strain	g_y	g_x	g_y	g_x
wild type[a]				
(−)	1.895	1.804	31	161
Stig	1.893	1.782	32	170
Ant	1.902	1.776	46	207
HQNO	1.893	1.794	38	226
1Ala				
(−)	1.897	1.804	44	204
Stig	1.893	1.782	31	171
Ant	1.904	1.802 (1.765)	50	205
HQNO	1.897	1.792	49	221
2Ala				
(−)	1.897	1.805	39	180
Stig	1.893	1.782	31	171
Ant	1.899	1.803 (1.770)	47	221
HQNO	1.897	1.803	37	212
3Ala				
(−)	1.897	1.801	33	130
Stig	1.894	1.779	41	179
Ant	1.897	1.801	33	131
HQNO	1.897	1.804	34	195
H212N				
(−)	1.899	1.803	48	200
Stig	1.894	1.781	31	172
Ant	1.903	1.799	50	209
HQNO	1.900	1.792	48	201
L286F				
(−)	1.897	1.803	38	204
Stig	1.894	1.782	31	170
Ant	1.902	1.775	48	210
HQNO	1.893	1.795	38	228

[a] Values were obtained as described (*20*).

inhibitors, antimycin A and HQNO, differently affected the angular dependence of the Fe/S protein EPR spectra.

Specificity of Antimycin A Induced Changes on the Mobility-Defective Fe/S Protein Mutants. The appearance of an entire new subset of Fe/S protein environments (with altered g_x maxima) upon the addition of a known Q_i site inhibitor like antimycin A led us to address to what extent this new [2Fe-2S] cluster environment was derived from any potential direct interaction with antimycin bound at the Q_o site. Similarly, to what extent the observation of a g_x' transition required the presence of a UQ at the Q_o site was also evaluated (Figure 3). First, the dependence of the g_x and g_x' transitions from the presence of a Q occupant at the Q_o site was tested using Q-depleted membranes from the +2Ala mutant. EPR spectra obtained using these samples indicated that upon Q extraction the $g_x = 1.805$ transition was replaced by another, still orientation-dependent $g_x = 1.782$ signal (Figure 3, top row). Second, no g_x' transition was seen upon addition of antimycin A to Q-depleted membranes of the +2Ala mutant derived samples (Figure 3, middle row). Third, addition of stigmatellin and antimycin A together to the native or the Q-extracted membranes yielded only a single g_x transition similar to that seen with stigmatellin alone (Figure 3, bottom rows). Together, these observations strongly correlated the g_x and g_x' transitions with a Q occupied Q_o site of the cyt bc_1.

Furthermore, whether the addition of antimycin A could affect directly the EPR spectrum of the Fe/S protein [2Fe-2S] cluster by its binding to the Q_o site was tested by examining light-activated cyt *b* reduction kinetics, as done earlier (*38*) (Figure 4). Addition of excess (approximately 20 μM instead of the routinely used 5 μM) antimycin A or HQNO did not abolish transient cyt *b* reduction or cyt *c* rereduction kinetics induced upon light activation of the reaction center. On the other hand, as a control, addition of myxothiazol completely abolished the kinetics by displacing the Q_o site occupant (Figure 4). Under the conditions used, neither antimycin A nor HQNO appeared to bind to the Fe/S protein or Q_o site to interfere with QH_2 oxidation in intact chromatophore membranes. The native-like cyt *b* reduction kinetics seen with both of the Q_i site inhibitors used here further supported the notion that the EPR g_x and g_x' transitions were not due to the binding of antimycin A to the Q_o, but rather to only the Q_i site.

Disruption of the Q_i Site by Elimination of Heme b_H in the +1Ala and +2Ala Mutants Also Revealed Dissimilar Effects of Antimycin A and HQNO Binding to Cyt bc_1. We have previously shown that cyt bc_1 mutants with a defective low potential chain, such as those lacking heme b_H (e.g., cyt *b*:H212N) or those affecting the stability of SQ at the Q_i site (e.g., cyt *b*:H217R), exhibited partially decreased angular dependence of the EPR spectra of their [2Fe-2S] clusters (*20*). Addition of antimycin A, but not HQNO, to these mutants further abolished the remaining angular dependence of the EPR spectra. These changes appeared to reflect the different modes of interactions of the inhibitors with the Q_i site rather than the changes in the redox states of the low potential chain components (*40*). Here the double mutants restricted for the Fe/S protein macromovement (*19*) and also lacking heme b_H of cyt bc_1 (*33, 41*) were examined (Figure 5). In the absence of any inhibitor, the +1Ala-bH212N and +2Ala-bH212N double mutants exhibited EPR spectra that are distinct from the native enzyme (*20*), the respective single mutants, and from one another (Figure 5A) (Tables 1 and 2). In particular, the EPR spectra of the reduced [2Fe-2S] cluster of the +2Ala-bH212N mutant were significantly broadened in the g_x transition region, and the g_y transition shifted to lower magnetic field positions. These spectral changes reflected the modified environments of the [2Fe-2S] clusters, combining the effects of the absence of heme b_H with the mobility restriction of the Fe/S proteins in the +*n*Ala mutants. The double mutant +1Ala-bH212N and +2Ala-bH212N EPR spectra still exhibited angular dependences similar to the single mutant cyt *b*:H212N (*20*). Thus, the contributions associated with restricting the Fe/S protein mobility (via the +*n*Ala mutations) were limited.

Addition of antimycin A to membrane samples from the +1Ala-bH212N and +2Ala-bH212N double mutants had significant effects on the width and spectral positions of the EPR transitions of the Fe/S protein [2Fe-2S] clusters of mutant enzymes (Table 2). Specifically, their EPR spectra were significantly broadened (Figure 5B), with the g_y and g_x transitions shifted to lower and higher magnetic field positions, respectively. However, no subpopulation exhibiting an EPR g_x' transition as seen previously with the single +1Ala and +2Ala mutants (Figure 2) was observed. Instead, only very broad g_x transitions (approximate $g_x = 1.783$) were visible, and the position of the observed transition maximum corresponded to neither the $g_x = 1.805$ nor those of the g_x' transitions of the +1Ala and +2Ala single mutants (Table 1). This indicated that an intact Q_i site containing the heme b_H was also needed for antimycin A to induce the two discrete [2Fe-2S] cluster subpopulations with distinct g_x and

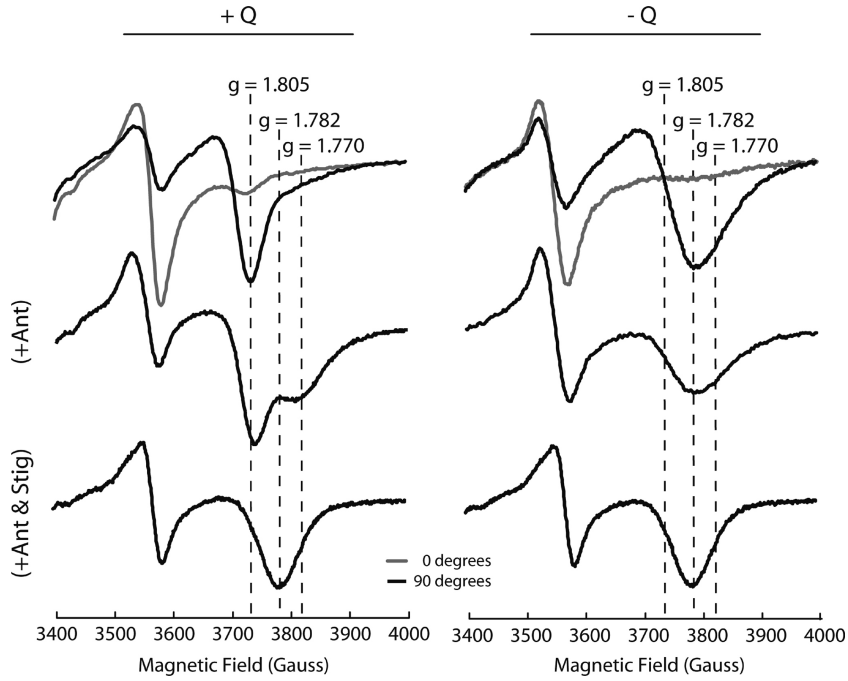

FIGURE 3: Orientation-dependent EPR spectra of the [2Fe-2S] cluster of ordered UQ-depleted membranes derived from the +2Ala cyt bc_1 containing strains treated with inhibitors. Ordered native (left) and UQ-depleted membranes (right) treated with antimycin A (+Ant, middle row) and with both antimycin A (10 μM) and stigmatellin (5 μM) (+Ant and Stig, bottom row) are presented. Spectra acquired at orientations versus the magnetic field where the g_y (gray traces) or g_x (black traces) transition amplitudes were maximal are shown on the top row. Spectrometer settings were as described in Figure 2.

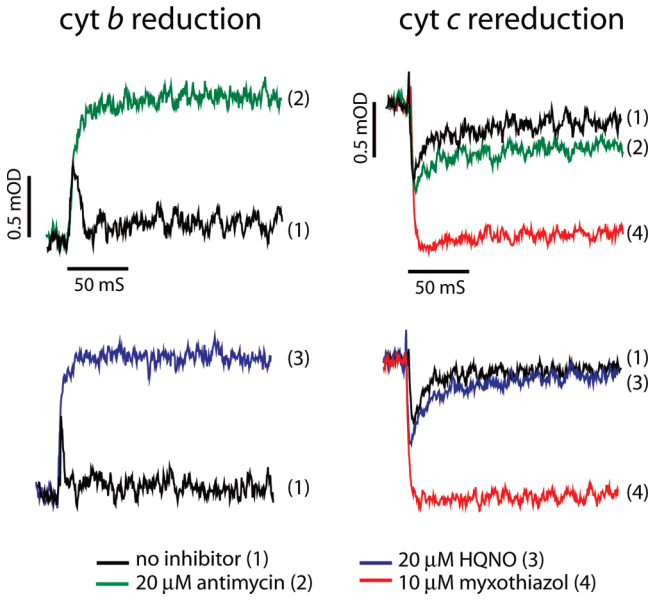

FIGURE 4: Light-induced, time-resolved cyt *b* reduction and cyt *c* rereduction kinetics of a wild-type *R. capsulatus* strain in the presence of various Q_o and Q_i site inhibitors. In each case, chromatophore membranes containing an amount of photochemical reaction center (RC) equal to 0.15 μM were resuspended in 50 mM MOPS buffer (pH 7.0) containing 100 mM KCl and 100 mM EDTA at an E_h of 100 mV. The amount of RC was determined based on the extent of its photooxidation by a train of 10 flashes separated by 50 ms at an E_h of 380 mV and using an extinction coefficient $\epsilon_{605-540}$ of 29 mM^{-1} cm^{-1}. The traces for cyt *b* reduction (left panel) were monitored at 560−570 nm in the absence (1, black traces) and the presence of the Q_i site inhibitor antimycin (20 μM) (2, green traces) or HQNO (20 μM) (3, blue traces), and those for cyt *c* rereduction (right panel) were monitored at 550−540 nm, in the absence and presence of the Q_o site inhibitor myxothiazol (10 μM) (4, red traces).

g_x' values in the +1Ala and +2Ala mutant cyt bc_1. Moreover, addition of antimycin A further decreased the angular dependence of the EPR spectra of these mutants, rendering them more similar to the quasi-random distribution of a similarly treated native enzyme. Although binding of antimycin A to the Q_i site still affected the mobility of the Fe/S protein, the mobility restrictions imposed by the +1Ala and +2Ala mutations were insufficient to reveal discrete subpopulations of Fe/S proteins, as if in the absence of heme b_H, the cyt bc_1 was conformation-wise more "relaxed".

For a complete comparison, spectral responses of the +1Ala-bH212N and +2Ala-bH212N double mutants to HQNO were also examined. The EPR spectra were similar to those seen with the single mutant parents, including the anisotropically broadened g_x and slightly shifted g_y transitions (Figure 5C). These changes were clearly different from those seen with antimycin A, especially with respect to the angular dependences of the EPR spectra, which were conserved in the presence of HQNO. Unlike antimycin A, the spectral effects induced by HQNO were less influenced by the absence of heme b_H, which is located directly adjacent to the Q_i site. Ordered EPR spectra derived from the Q_i mutants devoid of heme b_H further suggested that the [2Fe-2S] cluster EPR g_x and g_x' transitions seen upon exposure of the +1Ala and +2Ala mutants to antimycin A emanated from the constrained mobility of the Fe/S subunit.

The Cyt b ef Loop Mutation L286F Suppresses Antimycin A Induced Effects Seen by the EPR Spectra of the [2Fe-2S] Clusters in the +1Ala and +2Ala Mutants. If the appearance of the EPR g_x and g_x' transitions seen with the +1Ala and +2Ala mutants originated from the restricted mobility of the Fe/S proteins, then suppressor mutations improving the mobility defects might be expected to dissipate this finding.

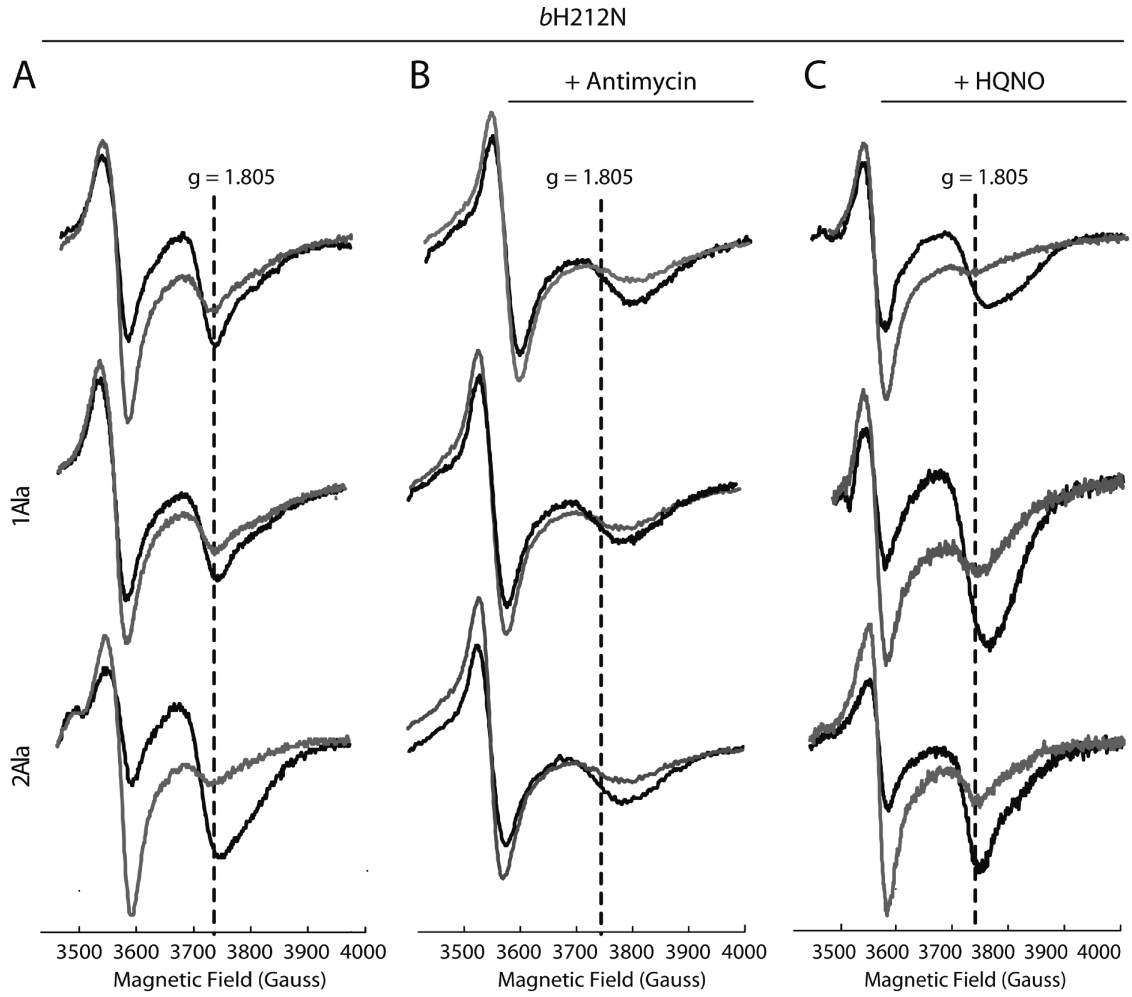

FIGURE 5: Orientation-dependent EPR spectra of the [2Fe-2S] cluster of the Fe/S protein using ordered membranes derived from the cyt *b*:H212N mutation containing +*n*Ala cyt bc_1 double mutants in the absence or presence of Q_i site inhibitors. Spectra obtained using ordered membranes from the cyt *b*:H212N single mutant (upper row, partly taken from ref *20*) and [+1Ala-bH212N] (middle row) and [+2Ala-H212N] (bottom row) double mutants in the absence of inhibitor (A, left) and in the presence of antimycin A (10 μM) (B, middle) or HQNO (30 μM) (C, right) are shown. Spectra acquired at orientations versus the magnetic field where the g_y (gray traces) or g_x (black traces) transition amplitudes were maximal are shown, and spectrometer settings were as described in Figure 2.

Table 2: EPR *g* Transition Positions and Spectral Widths from Various Double Mutant Ordered Membrane Samples

	transition maxima		transition width	
strain	g_y	g_x	g_y	g_x
1Ala::H212N				
(−)	1.897	1.805	46	203
Stig	1.893	1.783	30	175
Ant	1.898	1.781	48	210
HQNO	1.899	1.790	44	210
2Ala::H212N				
(−)	1.899	1.805	42	225
Stig	1.892	1.785	30	171
Ant	1.901	1.780	48	209
HQNO	1.898	1.803	44	211
1Ala::L286F				
(−)	1.896	1.804	36	211
Stig	1.893	1.782	32	170
Ant	1.894	1.783	32	175
HQNO	1.897	1.800	38	220
2Ala::L286F				
(−)	1.898	1.805	40	220
Stig	1.893	1.782	31	171
Ant	1.903	1.780	51	218
HQNO	1.895	1.799	37	225

Previously, we have shown that the cyt *b ef* loop L286F mutation decreased the mobility defect of the Fe/S protein in the +1Ala and +2Ala mutants (*19*). The L286F mutation is located at the apex of the cyt *b ef* loop, which is a direct extension of the transmembrane helix E, proposed to communicate the Q_i site occupancy state to the Q_o site (*20*). The basis of the slower movement in these mutants was attributed to physical hindrances imposed by the *ef* loop of cyt *b* on the macromobility of the Fe/S protein (*24*). Therefore, the +1Ala-bL286F and +2Ala-bL286F double mutants were examined for changes in the g_x and g_x' EPR transitions upon addition of antimycin A (Figure 6).

Ordered membrane samples from the single cyt *b*:L286F mutant indicated that the [2Fe-2S] cluster EPR spectra obtained in the absence of inhibitor or in the presence of antimycin A or HQNO (Figure 6, top row) were highly similar, though not identical, to those seen with a native enzyme (Figure 2). The maxima of the g_x transitions were located around $g = 1.805$, with the angular dependence of the EPR spectra being diminished in the presence of antimycin A but not with HQNO. The EPR spectra of the +1Ala-bL286F and +2Ala-bL286F double mutants in the absence of inhibitor were also different from one another, their respective single mutant parents, and the native cyt bc_1 (Figure 6A). However, the angular dependences of these

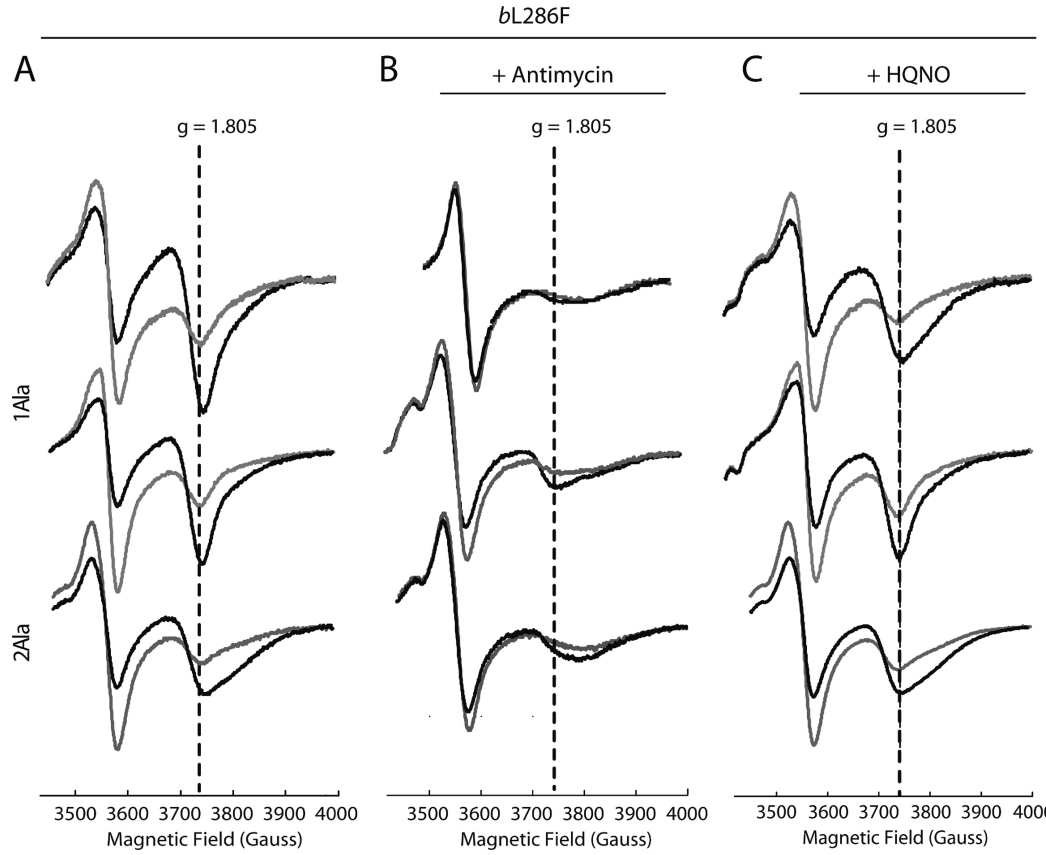

FIGURE 6: Orientation-dependent EPR spectra of the [2Fe-2S] cluster of the Fe/S protein using ordered membranes derived from the cyt *b*:L286F mutation containing +*n*Ala cyt bc_1 double mutants in the absence or presence of Q_i site inhibitors. Spectra obtained using ordered membranes from the cyt *b*:L286F single mutant (upper row) and [+1Ala-bL286F] (middle row) and [+2Ala-L286F] (bottom row) double mutants in the absence of inhibitor (A, left) and the presence of antimycin A (10 μM) (B, middle) or HQNO (30 μM) (C, right) are shown. Spectra acquired at orientations versus the magnetic field where the g_y (gray traces) or g_x (black traces) transition amplitudes were maximal are shown. Spectrometer settings were as described in Figure 2.

spectra, which were still detectable in the presence of HQNO, were attenuated in the presence of antimycin A. Moreover, in the +1Ala-bL286F or +2Ala-bL286F double mutants, the subpopulations exhibiting the EPR g_x and g_x' transitions induced by antimycin A addition to the +1Ala and +2Ala single mutants decreased or disappeared, respectively (Figure 6B). In the +1Ala-bL286F mutant, although the g_x and g_x' transitions could still be discerned, the ratio was dissimilar to that seen with the +1Ala single mutant (Figure 2). Furthermore, the EPR spectra of the +2Ala-bL286F mutant became very similar in the presence of antimycin A to those of the +2Ala-bH212N double mutant lacking heme b_H, exhibiting a single broad maximum located at $g = 1.783$ (Figure 5). Thus, in the double mutants, the disappearance of the g_x and g_x' transitions coincided with the suppression of the Fe/S protein mobility defects of the +*n*Ala mutants by the cyt *b ef* loop L286F mutation. This observation provided further support that the discrete Fe/S protein subpopulations correlated with the restricted mobility of this subunit of the cyt bc_1.

DISCUSSION

Conformational changes that occur in the cyt bc_1 in response to the binding of inhibitors to distant Q_o and Q_i sites are long known to occur, as described earlier by de Vries (*42*), Palmer (*43*), and Howell and Robertson (*44, 45*), examining the changing *b* heme spectroscopic properties as a function of inhibitor occupancies of the Q_o and Q_i sites of the cyt bc_1. More recent works extended these findings to include observations like substoichiometric quantities of Q_o site inhibitors to yield complete QH_2 oxidation inhibition (*31, 32, 46*) or increased proteolysis of the Fe/S protein in response to Q_i site inhibitors (*30*). These findings suggested regulatory communications between the Q_o and Q_i sites of each monomer, as well as between the two monomers of the cyt bc_1 (*20, 31, 47, 48*). Our previous work directly monitoring the changes in the [2Fe-2S] cluster and heme iron using orientation-dependent EPR spectroscopy indicated that the Q_i site inhibitors HQNO and antimycin A affected the Q_o and Q_i site communications in different ways (*20*). Both HQNO and antimycin A changed the EPR spectral line shapes, hence the immediate surroundings of the Fe/S subunit [2Fe-2S] clusters. However, only antimycin A dissipated the angular dependence of the EPR spectra, quasi-randomizing the distribution of the Fe/S protein within the cyt bc_1. As the structural data indicate that HQNO and antimycin A interact differently with the Q_i site boundaries (*7, 18*), we proposed that the former and latter inhibitors mimicked Q (possibly also SQ, i.e., a Q_i site ready to accept an electron) and QH_2 (or possibly empty, i.e., a Q_i site incompetent to accept an electron) at this site, respectively. Thus, the occurrence of different Q_i site intermediates is communicated continuously to the Q_o site to affect the Fe/S protein position to initiate QH_2 oxidation (*20*). In this work, we probed the Q_i-Q_o site coordination events using the Fe/S protein movement-defective mutants by directly monitoring their

[2Fe-2S] clusters via orientation-dependent EPR spectra. The data obtained here with the +*n*Ala mutants indicated that the decreased angular dependence of the Fe/S protein [2Fe-2S] cluster EPR spectra upon binding of antimycin A to native cyt bc_1 correlated well with the mobility of this subunit. No change in the angular dependence of the EPR spectrum of the macro- and micromobility-defective +3Ala mutant was observed. The macromovement-deficient +1Ala and +2Ala mutants exhibited different EPR spectra and revealed an additional subpopulation with the [2Fe2S] clusters at a g_x' magnetic field position distinct from the typical $g_x = 1.805$ transition. This subpopulation was not clearly seen with either the native cyt bc_1 or the immobile +3Ala mutant derivative. The appearance of this subpopulation was specific to antimycin A as it was absent in HQNO-treated or Q-depleted membrane samples. In addition, stigmatellin counteracted antimycin A mediated effects to dissipate both the g_x and g_x' transitions. Control experiments ruled out the possibility that antimycin A might act either directly on the Fe/S protein or at the Q_o site, leaving the possibility that these effects reflected Q_o-Q_i site communications. Earlier, binding of NQNO (an analogue of HQNO) to the Q_o site has been observed in a cyt bc_1 structure obtained using detergent-solubilized and purified enzyme (*18*). However, in no instance has binding of antimycin A to the Q_o site been reported, and based on our data, this inhibitor does not seem to do so with membrane-embedded enzyme either.

Sample Heterogeneity or Heterodimeric Enzyme? The finding that only the +1Ala and +2Ala mutants clearly exhibited two distinct subpopulations of [2Fe-2S] clusters upon exposure to antimycin A was remarkable. This observation suggested that either the membrane preparations used here were heterogeneous and contained two different kinds of dimeric cyt bc_1 subpopulations or the preparations were homogeneous but the two monomers of the cyt bc_1 were not identical. The fact that no pronounced heterogeneity was observed with HQNO, stigmatellin, Q-depleted samples, or the single cyt *b*:H212N and cyt *b*:L286F mutants or their +1Ala and +2Ala double mutant derivatives argues that membrane heterogeneity is not the culprit giving rise to the spectral heterogeneity. In addition, the fact that the mobility suppressor mutation cyt *b*:L286F dissipated the antimycin A induced heterogeneity seen with the +1Ala or +2Ala mutants further linked this heterogeneity to the interactions between the Fe/S protein and the cyt *b ef* loop, where this mutation is located, and provided further credence to the idea that the E helix plays a prominent role in the Q_o-Q_i communication. Similarly, absence of the two subpopulations in the double mutants +1Ala-bH212N and +2Ala-bH212N also lacking heme b_H and "relaxing" the cyt bc_1 conformation (*20, 30, 36*) suggested that absence of heme coordination between helices B and D of cyt *b* affected the conformation of the *ef* loop. In all of these cases, the *ef* loop ceased to act as a physical barrier for the Fe/S protein in the +1Ala and +2Ala mutants, increasing the quasi-random locations of this subunit within the cyt bc_1. Thus, binding of antimycin A revealed two [2Fe-2S] clusters of the Fe/S proteins with different immediate environments and implied that the two monomers of a dimeric cyt bc_1 might be asymmetric with respect to the conformations of their Fe/S proteins at the respective Q_o sites.

How the binding of antimycin A to an apparently symmetrical cyt bc_1 dimer can initiate asymmetry is not obvious. A plausible rationale is that the spectral heterogeneity documented here might originate from differently altered binding abilities of each of the two Q_i sites of the cyt bc_1. This would imply that, despite the saturating amounts of antimycin A, both of the Q_i sites were never fully occupied, yielding two subpopulations of Fe/S proteins with g_x and g_x' EPR transitions. However, adding antimycin A to a native enzyme or to the double +1Ala-bL286F and +2Ala-bL286F mutant sites did not induce two subpopulations, arguing against the hypothesis that there is a significant difference in antimycin A binding abilities of the two Q_i sites of a dimeric cyt bc_1. An additional hypothesis is that the observed heterogeneity is an intrinsic property of the resting native cyt bc_1 dimer, even in the absence of antimycin A, as seen in Figure 2 here, and also considered earlier by the "activated Q cycle" (*46*) and "half of the site, alternating enzyme" (*21, 49*) models. Thus, unless the Q_i sites are loaded with antimycin A, a fraction of the Fe/S proteins of the native cyt bc_1 might be in a different conformation at the Q_o sites so that only this fraction of the two [2Fe-2S] clusters contributes to the observed sharp EPR g_x 1.80 transition, while the remaining fraction yields a broader transition. This possibility is in line with the disappearance of the $g_x = 1.805$ transition of the native enzyme in the presence of antimycin A (*20*) and with the observations made with single crystal EPR spectroscopy, where orienting the *g* tensors of the clusters with their structural coordinates yielded two distinct Fe^{II} *g*-tensor orientations within a dimer (*50*). It is also consistent with the enhanced proteolysis of the Fe/S protein upon addition of antimycin A (*30*) and with full inhibition of the Q_o site catalysis upon use of substoichiometric amounts of stigmatellin (*51*). If this is the case, then binding of antimycin A to the Q_i sites of the +1Ala and +2Ala mutants would change the resting positions of the Fe/S protein [2Fe-2S] cluster in the Q_o sites, similar to that seen in the native enzyme. However, in the mobility-restricted +1Ala and +2Ala mutants, the [2Fe-2S] clusters would be differently "trapped" at the Q_o sites due to the longer Fe/S protein linker lengths and the ensuing physical interactions with the *ef* loop of cyt *b*, revealing two subpopulations with different g_x and g_x' transitions. This rationalization is consistent with the slower macromobilities and higher tendencies of the +1Ala and +2Ala mutant Fe/S proteins to reside at the Q_o site (*19, 52*). It predicts that the EPR g_x transition corresponding to the [2Fe-2S] cluster of a native cyt bc_1 might be substoichiometric as compared with the other cofactors.

No X-ray structure containing only antimycin A, without any additional inhibitor at the Q_o site, has so far been analyzed in detail. Most of the available structures containing antimycin A also contain another Q_o site inhibitor, like stigmatellin, which might override the effects of antimycin A (*7*). Even the high resolution cyt bc_1−cyt *c* cocrystal structures that exhibit remarkable asymmetry, with a single cyt *c* molecule bound to the dimeric cyt bc_1 and different Q_i site occupancies, still contain stigmatellin in the Q_o sites, limiting their use to assess the asymmetric behaviors of the Fe/S proteins (*9*). Preliminary comparisons of antimycin-inhibited and HQNO-inhibited enzymes lacking stigmatellin at the Q_o site indicate a potential difference in the distribution

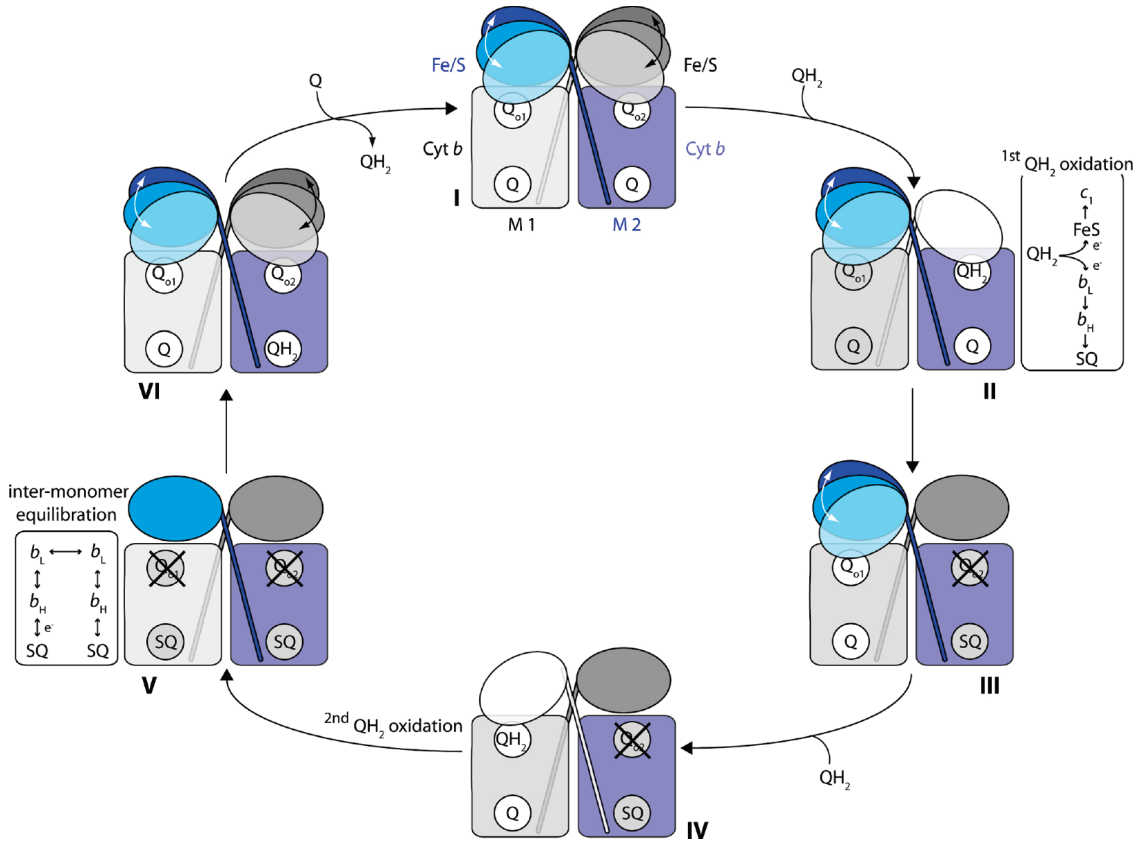

FIGURE 7: A working model for a complete turnover of a heterodimeric cyt bc_1. In stage I the two cyt *b* subunits of the two monomers (M1 and M2) of a dimeric cyt bc_1 are depicted as gray and purple rectangles, respectively. The cyt c_1 subunits are not shown for the sake of simplicity, and the multiple positions of the Fe/S protein extrinsic domain, shown as ellipses in shades of blue and black, respectively, are indicated with arrows. For each monomer, the Q_o and Q_i sites are drawn as circles and numbered as Q_{o1} and Q_{o2} for M1 and M2, respectively. The Q_i sites are shown to contain a Q; however, even if either or both of these sites were empty, it will be inconsequential for the subsequent events. At the onset, either monomer can catalyze QH_2 oxidation provided that their Q_i sites contain Q. Upon arrival of a QH_2 to a Q_o site (stage II) the Fe/S protein (e.g., that of M2 in white, overlapping QH_2 at the Q_{o2} site) catalyzes the first QH_2 oxidation, generating a SQ at the Q_{i2} site. The model assumes that while SQ resides at the Q_{i2} site, the corresponding Fe/S protein is unable to reach the Q_{o2} site following its oxidation by the cyt c_1 (e.g., due to the *ef* loop of cyt *b* acting as a barrier) (stage III). This forces the second QH_2 oxidation to occur obligatorily at the other Q_o site (i.e., Q_{o1} of M1) upon arrival of a QH_2 (stage IV). After completion of the second QH_2 oxidation, the two resulting SQ (stage V) are assumed to rapidly equilibrate via intermonomer electron transfer, to yield a Q and a QH_2 at the Q_i sites, and render the Fe/S proteins able to reach the Q_o sites (stage VI). As the intermonomer electron transfer can produce a QH_2 at either monomer, replacement of this QH_2 by a Q then returns the enzyme to stage I, where either monomer is able to initiate the next complete catalytic turnover.

of residues in the E helix as a function of binding of these inhibitors (Berry et al., manuscript in preparation).

A Heterodimeric Modified Q Cycle Model. Assuming that the native cyt bc_1 is a heterodimer with two asymmetric monomers, it is tempting to consider that the conformation of surface structures of cyt *b* at the Q_o site, including the *ef* loop and possibly *cd*1 and *cd*2 helices (*8, 34*), might provide a means to affect the location of the Fe/S protein via the Q_i site occupants. As binding of antimycin A (i.e., mimicking QH_2 or absence of Q) to the Q_i site, and not that of HQNO (i.e., mimicking Q or SQ), quasi-randomizes the location of Fe/S protein at the Q_o site, then stabilization of an SQ at the Q_i site could modify the conformation of the *cd* helices and *ef* loop via the E helix of cyt *b* (*20*). If so, following a QH_2 oxidation at a Q_o site, an oxidized Fe/S protein returning back to cyt *b* after conveying its electron to cyt c_1 might be shielded physically from reaching the catalytic portion of the Q_o site. No QH_2 oxidation at the same Q_o site could then occur as long as the Q_i site of that monomer contains a SQ, as depicted in Figure 7, leaving only the Q_o site of the other monomer competent for the next QH_2 oxidation. Accordingly, following a single turnover of each Q_o site of the dimeric cyt bc_1, each Q_i site would be occupied by a SQ species. Only upon intermonomer equilibration between the two low potential chains via the heme b_L of the monomers (*48, 53*) would two SQ yield a Q and a QH_2 at the two Q_i sites (Figure 7). This final state will render either Q_o site of the dimeric cyt bc_1 again competent to oxidize a QH_2 and initiate a new turnover. This mode of operation is different from an "alternating site model" where each Q_o site would alternate one after the other during multiple turnovers (*21, 49*). It rather follows the generally accepted modified Q cycle mechanism (*10, 23*) with two additional assumptions. First, the second QH_2 oxidation needed to convert the Q_i site SQ to a QH_2 is assumed to occur at the Q_o site of the other monomer. Second, it invokes the redox states of the low potential chains (*54*) and intermonomer electron transfer (*54, 55*). Consequently, it allows only one round of alternation of Q_o sites for a full catalytic turnover, leaving the possibility to initiate the next turnover at either Q_o site, rationalizing the functional importance of a dimeric cyt bc_1 structure (*4, 5*). This working model is consistent with the available data (*31, 32, 46*), but other interpretations are also conceivable (*23*). Its attractiveness, if any, stems from the ability to

accommodate the dimeric architecture of the cyt bc_1 with the need of two consecutive Q_o site turnovers via the modified Q cycle mechanism to account for a full catalytic cycle of cyt bc_1 (*1, 10, 11, 46, 56, 57*) (Figure 7). Hopefully, future studies, especially those teasing apart the characteristics of the two monomers of the cyt bc_1, will assess the validity of this and other related models.

REFERENCES

1. Berry, E. A., Guergova-Kuras, M., Huang, L. S., and Crofts, A. R. (2000) Structure and function of cytochrome *bc* complexes. *Annu. Rev. Biochem. 69*, 1005–1075.
2. Berry, E. A., Lee, D. W., Huang, L. S., and Daldal, F. (2008) Structural and mutational studies of the cytochrome bc_1 complex, in *The purple phototrophic bacteria* (Hunter, N. C., Daldal, F., Thurnauer, M. C., and Beatty, T. J., Eds.) pp 425−450, Springer, The Netherlands.
3. Kramer, D. M., Nitschke, W., and Cooley, J. W. (2008) The cytochrome bc_1 and related *bc* complexes: The Rieske/cytochrome *b* complex as the functional core of a central electron/proton transfer complex, in *The purple phototrophic bacteria* (Hunter, N. C., Daldal, F., Thurnauer, M. C., and Beatty, T. J., Eds.) pp 451−473, Springer, The Netherlands.
4. Xia, D., Yu, C. A., Kim, H., Xia, J. Z., Kachurin, A. M., Zhang, L., Yu, L., and Deisenhofer, J. (1997) Crystal structure of the cytochrome bc_1 complex from bovine heart mitochondria. *Science 277*, 60–66.
5. Zhang, Z., Huang, L., Shulmeister, V. M., Chi, Y. I., Kim, K. K., Hung, L. W., Crofts, A. R., Berry, E. A., and Kim, S. H. (1998) Electron transfer by domain movement in cytochrome bc_1. *Nature 392*, 677–684.
6. Berry, E. A., Huang, L. S., Saechao, L. K., Pon, N. G., Valkova-Valchanova, M., and Daldal, F. (2004) X-ray structure of *Rhodobacter capsulatus* cytochrome bc_1: comparison with its mitochondrial and chloroplast counterparts. *Photosynth. Res. 81*, 251–275.
7. Huang, L. S., Cobessi, D., Tung, E. Y., and Berry, E. A. (2005) Binding of the respiratory chain inhibitor antimycin to the mitochondrial bc_1 complex: a new crystal structure reveals an altered intramolecular hydrogen-bonding pattern. *J. Mol. Biol. 351*, 573–597.
8. Esser, L., Gong, X., Yang, S., Yu, L., Yu, C. A., and Xia, D. (2006) Surface-modulated motion switch: capture and release of iron-sulfur protein in the cytochrome bc_1 complex. *Proc. Natl. Acad. Sci. U.S.A. 103*, 13045–13050.
9. Solmaz, S. R., and Hunte, C. (2008) Structure of complex III with bound cytochrome *c* in reduced state and definition of a minimal core interface for electron transfer. *J. Biol. Chem. 283*, 17542–17549.
10. Crofts, A. R., and Meinhardt, S. W. (1982) A Q-cycle mechanism for the cyclic electron-transfer chain of *Rhodopseudomonas sphaeroides*. *Biochem. Soc. Trans. 10*, 201–203.
11. Osyczka, A., Moser, C. C., and Dutton, P. L. (2005) Fixing the Q cycle. *Trends Biochem. Sci. 30*, 176–182.
12. Cape, J. L., Bowman, M. K., and Kramer, D. M. (2006) Understanding the cytochrome *bc* complexes by what they don't do. The Q-cycle at 30. *Trends Plant Sci. 11*, 46–55.
13. Jenney, F. E., Jr., and Daldal, F. (1993) A novel membrane-associated *c*-type cytochrome, cyt c_y, can mediate the photosynthetic growth of *Rhodobacter capsulatus* and *Rhodobacter sphaeroides*. *EMBO J. 12*, 1283–1292.
14. Cape, J. L., Bowman, M. K., and Kramer, D. M. (2007) A semiquinone intermediate generated at the Q_o site of the cytochrome bc_1 complex: importance for the Q-cycle and superoxide production. *Proc. Natl. Acad. Sci. U.S.A. 104*, 7887–7892.
15. Zhang, H., Osyczka, A., Dutton, P. L., and Moser, C. C. (2007) Exposing the complex III Q_o semiquinone radical. *Biochim. Biophys. Acta 1767*, 883–887.
16. Zhu, J., Egawa, T., Yeh, S. R., Yu, L., and Yu, C. A. (2007) Simultaneous reduction of iron-sulfur protein and cytochrome b_L during ubiquinol oxidation in cytochrome bc_1 complex. *Proc. Natl. Acad. Sci. U.S.A. 104*, 4864–4869.
17. Darrouzet, E., Moser, C. C., Dutton, P. L., and Daldal, F. (2001) Large scale domain movement in cytochrome bc_1: a new device for electron transfer in proteins. *Trends Biochem. Sci. 26*, 445–451.
18. Esser, L., Quinn, B., Li, Y. F., Zhang, M., Elberry, M., Yu, L., Yu, C. A., and Xia, D. (2004) Crystallographic studies of quinol oxidation site inhibitors: a modified classification of inhibitors for the cytochrome bc_1 complex. *J. Mol. Biol. 341*, 281–302.
19. Darrouzet, E., and Daldal, F. (2002) Movement of the iron-sulfur subunit beyond the *ef* loop of cytochrome *b* is required for multiple turnovers of the bc_1 complex but not for single turnover Q_o site catalysis. *J. Biol. Chem. 277*, 3471–3476.
20. Cooley, J. W., Ohnishi, T., and Daldal, F. (2005) Binding dynamics at the quinone reduction (Q_i) site influence the equilibrium interactions of the iron sulfur protein and hydroquinone oxidation (Q_o) site of the cytochrome bc_1 complex. *Biochemistry 44*, 10520–10532.
21. Trumpower, B. L. (2002) A concerted, alternating sites mechanism of ubiquinol oxidation by the dimeric cytochrome bc_1 complex. *Biochim. Biophys. Acta 1555*, 166–173.
22. Covian, R., and Trumpower, B. L. (2008) Regulatory interactions in the dimeric cytochrome bc_1 complex: The advantages of being a twin. *Biochim. Biophys. Acta 1777*, 1079–1091.
23. Crofts, A. R., Holland, J. T., Victoria, D., Kolling, D. R., Dikanov, S. A., Gilbreth, R., Lhee, S., Kuras, R., and Kuras, M. G. (2008) The Q-cycle reviewed: How well does a monomeric mechanism of the bc_1 complex account for the function of a dimeric complex? *Biochim. Biophys. Acta 1777*, 1001–1019.
24. Darrouzet, E., and Daldal, F. (2003) Protein-protein interactions between cytochrome *b* and the Fe-S protein subunits during QH_2 oxidation and large-scale domain movement in the bc_1 complex. *Biochemistry 42*, 1499–1507.
25. Xia, D., Esser, L., Yu, L., and Yu, C. A. (2007) Structural basis for the mechanism of electron bifurcation at the quinol oxidation site of the cytochrome bc_1 complex. *Photosynth. Res. 92*, 17–34.
26. Tian, H., Yu, L., Mather, M. W., and Yu, C. A. (1998) Flexibility of the neck region of the rieske iron-sulfur protein is functionally important in the cytochrome bc_1 complex. *J. Biol. Chem. 273*, 27953–27959.
27. Tian, H., White, S., Yu, L., and Yu, C. A. (1999) Evidence for the head domain movement of the rieske iron-sulfur protein in electron transfer reaction of the cytochrome bc_1 complex. *J. Biol. Chem. 274*, 7146–7152.
28. Ma, H. W., Yang, S., Yu, L., and Yu, C. A. (2008) Formation of engineered intersubunit disulfide bond in cytochrome bc_1 complex disrupts electron transfer activity in the complex. *Biochim. Biophys. Acta 1777*, 317–326.
29. Gray, K. A., Dutton, P. L., and Daldal, F. (1994) Requirement of histidine 217 for ubiquinone reductase activity (Q_i site) in the cytochrome bc_1 complex. *Biochemistry 33*, 723–733.
30. Valkova-Valchanova, M., Darrouzet, E., Moomaw, C. R., Slaughter, C. A., and Daldal, F. (2000) Proteolytic cleavage of the Fe-S subunit hinge region of *Rhodobacter capsulatus* bc_1 complex: effects of inhibitors and mutations. *Biochemistry 39*, 15484–15492.
31. Covian, R., Gutierrez-Cirlos, E. B., and Trumpower, B. L. (2004) Anti-cooperative oxidation of ubiquinol by the yeast cytochrome bc_1 complex. *J. Biol. Chem. 279*, 15040–15049.
32. Covian, R., and Trumpower, B. L. (2006) Regulatory interactions between ubiquinol oxidation and ubiquinone reduction sites in the dimeric cytochrome bc_1 complex. *J. Biol. Chem. 281*, 30925–30932.
33. Osyczka, A., Moser, C. C., Daldal, F., and Dutton, P. L. (2004) Reversible redox energy coupling in electron transfer chains. *Nature 427*, 607–612.
34. Darrouzet, E., Valkova-Valchanova, M., Moser, C. C., Dutton, P. L., and Daldal, F. (2000) Uncovering the [2Fe2S] domain movement in cytochrome bc_1 and its implications for energy conversion. *Proc. Natl. Acad. Sci. U.S.A. 97*, 4567–4572.
35. Atta-Asafo-Adjei, E., and Daldal, F. (1991) Size of the amino acid side chain at position 158 of cytochrome *b* is critical for an active cytochrome bc_1 complex and for photosynthetic growth of *Rhodobacter capsulatus*. *Proc. Natl. Acad. Sci. U.S.A. 88*, 492–496.
36. Cooley, J. W., Roberts, A. G., Bowman, M. K., Kramer, D. M., and Daldal, F. (2004) The raised midpoint potential of the [2Fe2S] cluster of cytochrome bc_1 is mediated by both the Q_o site occupants and the head domain position of the Fe-S protein subunit. *Biochemistry 43*, 2217–2227.
37. Brugna, M., Rodgers, S., Schricker, A., Montoya, G., Kazmeier, M., Nitschke, W., and Sinning, I. (2000) A spectroscopic method for observing the domain movement of the Rieske iron-sulfur protein. *Proc. Natl. Acad. Sci. U.S.A. 97*, 2069–2074.
38. Lee, D. W., Ozturk, Y., Osyczka, A., Cooley, J. W., and Daldal, F. (2008) Cytochrome bc_1-c_y fusion complexes reveal the distance

constraints for functional electron transfer between photosynthesis components. *J. Biol. Chem. 283*, 13973–13982.
39. Ding, H., Robertson, D. E., Daldal, F., and Dutton, P. L. (1992) Cytochrome bc_1 complex [2Fe-2S] cluster and its interaction with ubiquinone and ubihydroquinone at the Q_o site: a double-occupancy Q_o site model. *Biochemistry 31*, 3144–3158.
40. Drose, S., and Brandt, U. (2008) The mechanism of mitochondrial superoxide production by the cytochrome bc_1 complex. *J. Biol. Chem. 283*, 21649–21654.
41. Hacker, B., Barquera, B., Crofts, A. R., and Gennis, R. B. (1993) Characterization of mutations in the cytochrome *b* subunit of the bc_1 complex of *Rhodobacter sphaeroides* that affect the quinone reductase site (Q_c). *Biochemistry 32*, 4403–4410.
42. de Vries, S. (1986) The pathway of electron transfer in the dimeric QH_2: cytochrome *c* oxidoreductase. *J. Bioenerg. Biomembr. 18*, 195–224.
43. Tsai, A. L., Kauten, R., and Palmer, G. (1985) The interaction of yeast Complex III with some respiratory inhibitors. *Biochim. Biophys. Acta 806*, 418–426.
44. Robertson, D. E., Giangiacomo, K. M., de Vries, S., Moser, C. C., and Dutton, P. L. (1984) Two distinct quinone-modulated modes of antimycin-sensitive cytochrome *b* reduction in the cytochrome bc_1 complex. *FEBS Lett. 178*, 343–350.
45. Howell, N., and Robertson, D. E. (1993) Electrochemical and spectral analysis of the long-range interactions between the Q_o and Q_i sites and the heme prosthetic groups in ubiquinol-cytochrome *c* oxidoreductase. *Biochemistry 32*, 11162–11172.
46. Mulkidjanian, A. Y. (2007) Proton translocation by the cytochrome bc_1 complexes of phototrophic bacteria: introducing the activated Q-cycle. *Photochem. Photobiol. Sci. 6*, 19–34.
47. Yu, C. A., Wen, X., Xiao, K., Xia, D., and Yu, L. (2002) Inter- and intra-molecular electron transfer in the cytochrome bc_1 complex. *Biochim. Biophys. Acta 1555*, 65–70.
48. Gong, X., Yu, L., Xia, D., and Yu, C. A. (2005) Evidence for electron equilibrium between the two hemes b_L in the dimeric cytochrome bc_1 complex. *J. Biol. Chem. 280*, 9251–9257.
49. Snyder, C. H., Gutierrez-Cirlos, E. B., and Trumpower, B. L. (2000) Evidence for a concerted mechanism of ubiquinol oxidation by the cytochrome bc_1 complex. *J. Biol. Chem. 275*, 13535–13541.
50. Bowman, M. K., Berry, E. A., Roberts, A. G., and Kramer, D. M. (2004) Orientation of the g-tensor axes of the Rieske subunit in the cytochrome bc_1 complex. *Biochemistry 43*, 430–436.
51. Gutierrez-Cirlos, E. B., and Trumpower, B. L. (2002) Inhibitory analogs of ubiquinol act anti-cooperatively on the yeast cytochrome bc_1 complex. Evidence for an alternating, half-of-the-sites mechanism of ubiquinol oxidation. *J. Biol. Chem. 277*, 1195–1202.
52. Crofts, A. R., Guergova-Kuras, M., Kuras, R., Ugulava, N., Li, J., and Hong, S. (2000) Proton-coupled electron transfer at the Q_o site: what type of mechanism can account for the high activation barrier? *Biochim. Biophys. Acta 1459*, 456–466.
53. Covian, R., Zwicker, K., Rotsaert, F. A., and Trumpower, B. L. (2007) Asymmetric and redox-specific binding of quinone and quinol at center N of the dimeric yeast cytochrome bc_1 complex. Consequences for semiquinone stabilization. *J. Biol. Chem. 282*, 24198–24208.
54. Brandt, U. (1996) Energy conservation by bifurcated electron-transfer in the cytochrome-bc_1 complex. *Biochim. Biophys. Acta 1275*, 41–46.
55. Shinkarev, V. P., and Wraight, C. A. (2007) Intermonomer electron transfer in the bc_1 complex dimer is controlled by the energized state and by impaired electron transfer between low and high potential hemes. *FEBS Lett. 581*, 1535–1541.
56. Trumpower, B. L. (1990) The protonmotive Q cycle. Energy transduction by coupling of proton translocation to electron transfer by the cytochrome bc_1 complex. *J. Biol. Chem. 265*, 11409–11412.
57. Link, T. A. (1997) The role of the "Rieske" iron sulfur protein in the hydroquinone oxidation (Q_P) site of the cytochrome bc_1 complex. The "proton-gated affinity change" mechanism. *FEBS Lett. 412*, 257–264.

BI802216H